WPS1-CPR(17) 18006

V Winters et al.

Overview of the initial plasma-surface interaction processes found in start-up plasmas of W7-X

Preprint of Paper to be submitted for publication in Proceeding of 16th International Conference on Plasma-Facing Materials and Components for Fusion Applications

This work has been carried out within the framework of the EUROfusion Consortium and has received funding from the Euratom research and training programme 2014-2018 under grant agreement No 633053. The views and opinions expressed herein do not necessarily reflect those of the European Commission.

Overview of the plasma-surface interaction analysis in the limiter phase of W7-X

V. R. Winters[1], S. Brezinsek[2], F. Effenberg[1], M. Rasinski[2], O. Schmitz[1], L. Stephey[1], C. Biedermann[3], C. P. Dhard[3], H. Frerichs[1], J. Harris[4], M. Krychowiak[3], R. König[3], T. Sunn Pedersen[3], G. A. Wurden[5], and the W7-X Team

[1]University of Wisconsin-Madison, Madison, WI, 53706 USA
[2]Forschungszentrum Jülich GmbH, IEK-4, 52425 Jülich, Germany
[3]Max-Planck-Institut für Plasmaphysik, 17491 Greifswald, Germany
[4]Oak Ridge National Laboratory, Oak Ridge, TN, 37830 USA
[5]Los Alamos National Laboratory, Los Alamos, NM, 87545 USA

E-mail: `vrwinters@wisc.edu`

May 2017

Abstract. The first operational campaign of Wendelstein 7-X (W7-X) provided an excellent environment for the study of plasma-surface interaction in a 3D stellarator. In-situ spectroscopic analysis via a combined visible/infrared camera system and a filterscope system revealed that the primary erosion zone was correlated with the high heat flux regions on the limiter. This analysis matched to where the erosion zone was found in the post-mortem analysis, which was done with SEM/FIB/EDX imaging. Additionally, a region of prompt deposition was found to the inside of these high heat flux zones. A region of far SOL deposition was found at the edges of the limiter tiles. All deposition regions were identified by their homogenious, increased oxygen content compared to the pure carbon makeup of the limiters. Poloidal variation of the impinging heat flux follow the imprint of the 3D scrape-off layer (SOL) flux tubes. In how far this reflects in the plasma-surface interaction will require further analysis and modeling.

Submitted to: *Phys. Scr.*

1. Introduction

Plasma-surface interaction (PSI) in magnetically confined fusion plasmas, though relatively well-studied in axi-symmetric environments such as in tokamaks [1], still needs dedicated research in the presence of 3D plasma edge topologies. Knowledge of how impurities are produced from plasma-facing components is especially important for the 3D topologies generated in stellarators in case they have a negative radial electric field in the edge, which can draw impurities into the core [2]. With an understanding of the underlying physics of the PSI, predictive modeling of the impurity sourcing to the core as well as ways of mitigating the erosion source can be developed.

The 3D environment present in the first operational campaign of Wendelstein 7-X (W7-X) was an excellent test bed for an initial understanding of its PSI with graphite based plasma-facing components (PFCs) [3]. The majority of experiments were performed in the same magnetic configuration with PSI localised at the 5 graphite poloidal limiter beams, which makes erosion and deposition patterns easier to interpret and relate to the operational conditions. In addition, the main plasma-facing components, the limiters, were taken out immediately after the initial operational phase of 311s stellarator plasma exposure [4], and all are available to be analyzed by ex-situ methods.

Field line tracing allows the study of the 3D magnetic structure of the scape-off layer domain as a basis to address 3D PSI aspects in the startup configuration at W7-X. A helically-shaped scrape-off layer (SOL) is revealed as shown in Figure 1. The SOL is comprised of three primary magnetic flux tubes (Figure 1a) in the poloidal map of the magnetic connection length L_c and by tracing a representative field line in each flux tube (Figure 1b). One flux tube completes exactly one full toroidal turn before hitting the same limiter, $L_c = 36m$, one makes one full toroidal turn but hits the next neighboring limiter $L_c = 42m$, and one completes two full toroidal turns and hits the next neighboring limiter $L_c = 80m$. These three magnetic flux tubes then form the magnetic footprint pattern seen in Figure 1c and they define the plasma surface interaction. Modeling results of the 3D transport features as well as heat and particle fluxes onto the limiters are discussed in detail in [5]. In this paper, a first systematic analysis of experimental data on the PSI on the limiters in this configuration is presented. The observation and analysis region (the diagnostic line-of-sight) is the boxed region and the dashed line represents the location of the post-mortem analysis region in Figure 1.

Modeling results from EMC3-EIRENE [5], which included a fixed intrinsic carbon source, indicate that the heat and particle loads are expected to correlate with the magnetic connection length footprint on the limiter. While the experimentally observed heat load distribution measured by infrared thermography were confirmed to match to the predicted distribution modeled by EMC3-EIRENE [6], as seen in Figure 2a and b, the poloidal variation of the Hydrogen particle flux distribution do not match to that predicted by EMC3-EIRENE seen in Figure 2c and d. The reason for this is still being investigated and whether the PSI shows any poloidal variation from the magnetic flux tube geometry is still the subject of ongoing research [7].

In this paper, an overview is presented of the spectroscopic measurements made on the limiters before materials analysis was completed and their connection to the post-mortem materials analysis that has been done so far. In addition, the physics processes assumed to be the cause of the main features on each limiter are introduced as well as a comparison of the features on the different limiters.

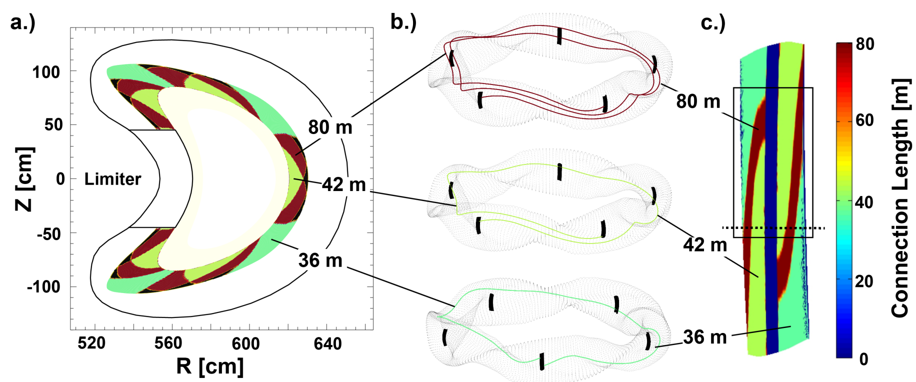

Figure 1. Visualization of the 3D flux tube geometry of the helical scrape-off layer of W7-X for OP1.1 plasmas. (a) A poloidal slice of the target-to-target magnetic connection lengths L_c in the bean shaped cross-section, where the limiters were located. (b) A 3D representation of the primary flux tube bundles, which cause the magnetic connection length footprint on the limiters (c).

2. Experimental Set-Up

During its first operational campaign, the W7-X stellarator was fitted with five poloidal limiters [3], each comprised of 9 fine grain graphite tiles, placed in stellarator-symmetric locations in the bean-shaped plane on the inboard side, as seen in Figure 1a. Tiles 3 and 7 of Limiter 5 contained sets of Langmuir Probes [8], which provided local plasma electron temperature and density measurements. A camera system which splits visible and infrared light by a germanium beam splitter from LANL [9], provided predominately a view of the Hα(656.3nm) photon flux on tiles 2-6 of Limiter 3 and limiter surface temperature/heat flux maps along the same line of sight. Limiter 3 was also fitted with an ORNL filterscope system [10], which provided integrated photon flux measurements of H_α (656nm), H_β (486nm), He-I (667nm) and C-II (514.5nm) emission observing tiles 3 and 4. Detailed information on these camera systems and interference filters can be found in [6], [11].

2.1. Spectroscopy

Photon fluxes from the filterscope system and the visible camera systems described in Section 2 can be converted to a particle flux via an S/XB coefficient [12], provided that the local plasma parameters where the light is being emitted are known and their

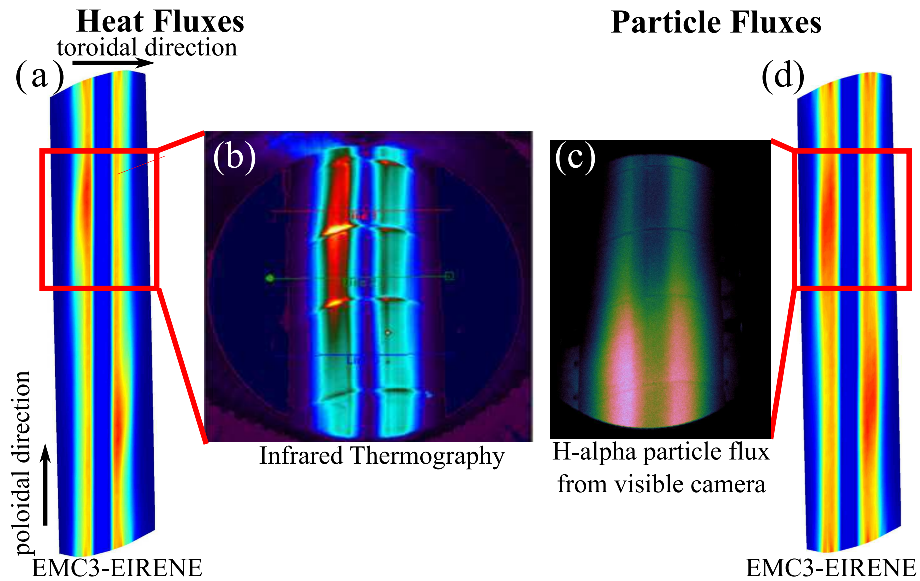

Figure 2. EMC3-EIRENE predictions of the heat flux (a), match to the surface temperature distribution that was seen in experiment (b) [6]. However, the experimental particle flux (c), does not match poloidally to EMC3-EIRENE predictions (d). It appears as though the experimental particle flux has a different poloidal dependency to the modeling, however the toroidal dependence appears to correspond to the modeling predictions. Each full limiter is about 16cm thick toroidally and 1m tall poloidally. The camera sees about 1/3 of the full limiter.

gradients not too large. These local plasma parameters T_e and n_e will be determined from limiter langmuir probe data, which will be discussed below.

At the given particle flux densities at the limiter, the surface of the graphite is almost saturated and the hydrogen recycling coefficient almost one, thus the vast majority of impinging protons is recycled and released as thermal hydrogen molecules which are subsequently dissociated and ionised. The hydrogen Balmer light is therefore a proxy for the impinging proton flux on on the graphite surface [13] considering the molecular correction. Therefore, a theoretical eroded carbon flux can be extracted from a hydrogen atomic particle flux measurement. This atomic recycling flux obtained from the filtered visible camera or filterscope can then be used as an effective proton flux with a sputtering yield calculation shown in Equation 1 that includes contributions from chemical and physical sputtering of graphite. The chemical sputtering yield is calculated by a formula determined by Roth [1], whereas the physical sputtering yield is determined from TRIM calculations and an average impact angle of incidence of 60 degrees [14].

$$\phi_C = (Y_{chem} + Y_{phys})\phi_H = (\frac{Y_{low}(E, T_{surf})}{1 + (\phi_H/6.0 \times 10^{21})^{.54}} + Y_{phys})\phi_H \tag{1}$$

In Equation 1, $Y_{low}(E, T_{surf})$ refers to the chemical erosion yield at low flux values, which is dependent on the impact energy of the ion, E, and the surface temperature of the limiter T_{surf}. Ion impact energy is determined using the assumptions that the impact energy is 5 times the plasma temperature of the ions and that the electron temperature is equal to the ion temperature [15]. Using the H-alpha recycling flux for this calculation is valid under the assumption that the atomic recycling flux is dominant.

Converting from a line-integrated photon flux to a particle flux requires some assumptions. The limiter n_e and T_e values are used since it is assumed that this is the region where the majority of emission is generated. We assume that the local plasma conditions at the spectroscopic location (Limiter 3) are equal to the ones at the location of the Limiter Langmuir probes (Limiter 5) However, we are aware that the heat flux received by Limiter 5 and Limiter 3 were slightly different, with Limiter 3 receiving an overall lower heat flux [6], and therefore some uncertainty with the similarities between the local plasma parameters of these two limiters are introduced. The error in these calculations take into account an error of a factor of 2 in temperature measurements, with the measurements from Limiter 5 taken as an upper bound. Errors due to a factor of 2 difference in density were negligible compared to the effect of temperature and were therefore ignored in these calculations.

According to the Limiter Langmuir Probe measurements, $T_e \approx 25$eV, $n_e \approx 2 \times 10^{18}\mathrm{m}^{-3}$ outside of the high heat and particle flux regions, shown in blue in Figure 2, while $T_e \approx 50$eV, $n_e \approx 3.5 \times 10^{18}$ m^{-3} within the high heat and particle flux regions. This difference in temperature does not affect the yield at low flux values by much, as seen from data in [16]. The limiter surface temperature is determined experimentally from the IR camera, and was found to vary between 400-500K across the entire limiter, which is not a large enough difference to affect the chemical erosion yield significantly. The approximate sputtering yield at low flux values for parameters similar to the ones at W7-X was found to be $Y_{low} = .01$, from data in [16]. The total sputtering yields used in this paper exclude any sputtering from impurities like oxygen, meaning $Z_{eff} = 1$ is assumed. Effects of impurities with $Z_{eff} \neq 1$will be considered in future work.

2.2. Post-Mortem Analysis

Tiles from 3 different limiters, each receiving different levels of heat flux, were analyzed, and are labeled as I-IV in Figure 3. The cuts removed a horizontal strip from the middle of each tile, and that horizontal strip was cut into 6 equally sized pieces in order to perform Scanning Electron Microscopy (SEM), Focused Ion Beam (FIB) and Electron Dispersive X-Ray Spectroscopy (EDX) analysis. All 6 pieces of Limiter 4, Tile 6 were analyzed to see if there were strong left-right asymmetries in the tile. Other limiter tiles were analyzed on one-half side only.

The SEM is used to view directly the surface of each sample. The FIB is a Galium beam that is used to cut into a small section of the sample. In order to preserve the surface structure, which can be coated in material that was eroded by the Galium beam, a small layer of Platinum was deposited on the area of interest before cutting. This small cross-section of the sample can then be viewed with the SEM and EDX to determine surface layer thickness and composition.

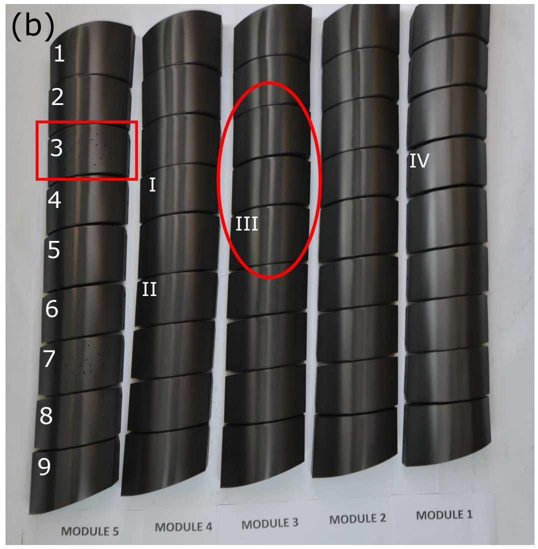

Figure 3. The layout of all limiter tiles after exposure to the OP1.1 plasmas. The numbers 1-9 represent how the tiles were numbered on the limiters. The boxed tile is Limiter 5, Tile 3 and is where local plasma parameters were measured for the analyses contained in this paper. The red oval shows the view that the visible camera/IR system had. And the roman numeral numbered tiles were all of the tiles that have been analyzed as of this writing.

EDX analysis determines the chemical composition of a region of interest by the detection of characteristic X-rays that are released by excited atoms in the material. These atoms are excited by the electron probe in the SEM. EDX was used both on the top uncut surface of the sample and on the cut surfaces in order to get a chemical analysis of the surface and also the thickness of the deposition coatings. The voltage of the electron beam in the SEM was varied between 5-15keV to determine both light and heavy impurities in the material.

In addition to the SEM/FIB/EDX analysis discussed here, Laser-Induced Breakdown Spectroscopy (LIBS) [17] measurements were done in order to measure the Hydrogen content of the surface of the samples.

3. Results

3.1. Spectroscopy Results

The spatial distribution of the Hydrogen particle flux deduced from spectroscopy (2.1) is shown in Figure 2c. The deduced spatial distribution of eroded carbon flux assuming a total carbon erosion yield according to Equation 1 and the impinging ion flux distribution according to Figure 2c is depicted in Figure 4. It is apparent that the primary carbon net erosion area, characterized by the higher carbon particle flux, is concentrated toroidally on the area that receives the highest heat and proton particle fluxes. It is important to note that for both the filterscope measurements, two S/XB coefficients were used for the C-II light; one in the main SOL (S/XB=55) and one in the far SOL (S/XB=23). The S/XB coefficients for the H_α photon flux was multiplied by a factor of 2 from the one in found in the ADAS database in order to account for molecular processes as mentioned before [13]. The reason for this is that the plasma parameters were relatively constant along the limiter with the exception of the main heat flux channels, which tended to have an electron temperature twice that of the areas outside of the channels, as seen in Section 2.1. In addition, two physical sputtering coefficients were used in 1, one in the main SOL ($Y_{phys} = .02$) and one in the far SOL $Y_{phys} = .013$. These physical sputtering coefficients were smoothed between the zones using sigmoid functions to avoid unphysical gradients in the carbon flux distribution. Compared to modeling, the particle load matches to what was expected from modeling in the toroidal direction, however poloidally the particle fluxes are not seen to agree with results from EMC3-EIRENE [5]. So far, the reason for this remains unclear[7].

Because there was no direct experimental measurement of the spatial CII photon flux distribution on any of the limiters, the integrated CII photon fluxes from the filterscopes were used for comparison with the calculated C fluxes on the basis of the Balmer emission. The result is shown in Figure 5. Here the shaded areas correspond to the range of values that the particle fluxes could be with experimental uncertainty included. The carbon particle flux determined from the C-II light from the filterscope agrees, to within these experimental uncertainties, with the carbon particle flux extracted from the filterscope Hα signal. Therefore, the sputtering formula can be used to extract the intrinsic eroded carbon source.

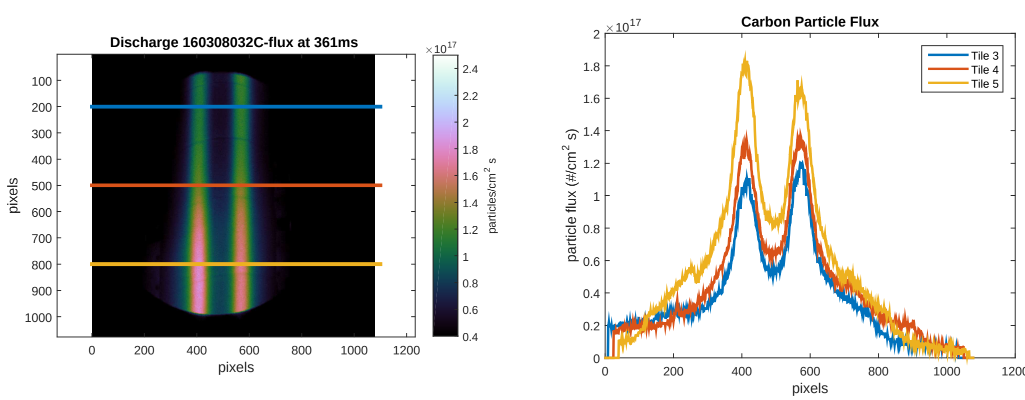

Figure 4. Map of the resulting eroded carbon flux found from using the Hα particle flux in Equation 1. Three lineouts are taken at various vertical limiter locations. The flux increases towards the bottom of the viewing area of the camera. The majority of the carbon flux toroidally is located in the zones of high heat flux.

3.2. Post-Mortem Materials Analysis Results

A general sketch of the expected physics processes contributing to the features of each limiter tile are shown in Figure 6, while the main features observed on the limiters are shown in Figure 7. Upon inspection of the four different tiles on three different limiters,

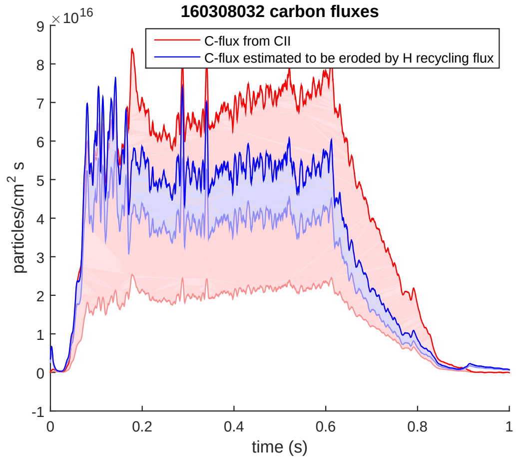

Figure 5. Comparison of the carbon particle flux as determined by C-II light versus the carbon particle flux as determined from the H-alpha light. The measurements agree to within experimental error, which is shown by the shaded areas for each measurement.

shown in Figure 3, in conjunction with the intrinsic spectroscopic measurements, 4 main zones with presumably underlying PSI processes were identified. The first region, labeled 1 on Figure 6 is the very center of the limiter, where the magnetic field lines of the LCFS are tangent to the surface. What was seen on the surface, as shown in Figure 7c, was a smoothening of the original surface structure, shown in 7a. This is believed to be from low-flux plasma wetting from cross-field transport. No impurities were found on the very center from EDX analysis, making it a very moderate net erosion zone.

The second area, labeled 2 on Figure 6, appears as 2 dull stripes just offset from the center in photographs. These dull stripes are labeled as 2 in Figure 7b, and SEM imaging of the surface, Figure 7d, show a rough surface. By cutting the surface with the FIB and subsequently doing an EDX map on the cross section, rough porous deposits were found. The deposits are visualized from the EDX chemical mapping as a decrease in Carbon content and homogeneous increase in Oxygen content. Figure 8b and c show the chemical map of the part of the FIB-cut cross section shown in Figure 8a, that is boxed. The high porosity of the deposit, visualized in Figure 8a, and that the deposit is not evenly coating the surface of the limiter in this section, suggests that the deposits did not originate from pure SOL background plasma deposition. It is more likely to be formed from local effects, such as erosion with local redeposition together with oxygen ions and protons from the plasma.

Directly next to these dull stripes is the section labeled 3 on Figure 6 and is where the tile received the majority of the heat and particle flux. This is a net erosion zone which provides the majority of the C found in the plasma. Closest to the dull stripes, there was no evidence of deposition. However, a smooth deposition layer gradually develops across the surface of the limiter out to the very edge of the tile. An example can be seen in Figure 9. Unlike the rough, porous deposits that were seen in Figure 8, the deposits appear as a smooth and dense, even coating on the limiter up to μm thickness. This layer also has a high fraction of embedded hydrogen [17]. This is seen in Figure 9a. The corresponding EDX chemical composition maps, Figure 9b and c, again show the decreased carbon content and the increased oxygen content that is used to characterize where the surface deposition layer is. This smooth, even coating on the limiter is characteristic of far SOL, global background plasma deposition. It was found that the layer gradually increases from center-to-edge to approximately 1μm, however decreases at the very edge of the limiter to about 300-400nm, causing the colorful a-C:H layer at the surface of 3-4 orders.

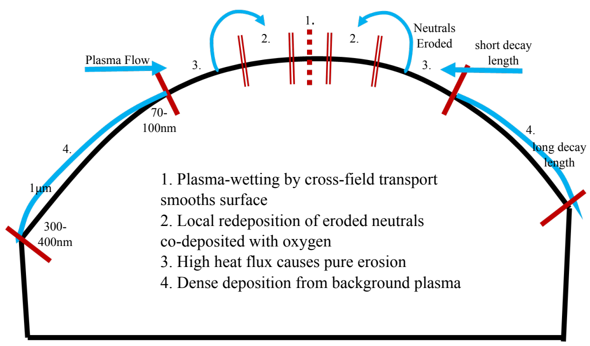

Figure 6. A schematic overview of the plasma-material interaction processes that occurred on the W7-X graphite limiters.

Evidence for the assertion that the rough, porous deposits were generated by local redeposition is shown in Figure 10. The left-side image is an SEM photo of the surface, which shows sand dune-like structures oriented horizontally across the limiter surface, pointing towards a plasma flow which flowed toroidally across the limiter. The right side of Figure 10 also shows a photo of Limiter 5, Tile 7. The holes containing the Langmuir probes can be seen to have features pointing towards the center of the limiter. It is believed that the flow of the background plasma on the sputtered neutrals in the high heat flux primary erosion zone would push the neutrals overall towards the center of the limiter. These neutrals would then be locally redeposited onto the surface, creating the rough stripes. By contrast, outside edges of the limiter are deeper in the scrape-off layer and are not subject to large amounts of erosion. Therefore, the far SOL, cooler plasma generates a net smooth, dense deposition layer with high hydrogen content [17].

All limiter tiles show the four main interaction zones outlined in Figure 6. Figure 11 shows a comparison between three tiles on three different limiters which had varying levels of heat flux [6]. It is important to note, however, that while all tiles had the same interaction zones, the size of these zones vary among limiters. For example, although Limiter 1 also had a region of rough deposits, it was much thinner than those found on the other limiters. This is likely due to Limiter 1 receiving about twice the heat flux as the other limiters [18]. This higher heat flux could have eroded more of these deposits on Limiter 1.

EDX scans of the limiter surface reveal that the main impurities deposited on the surface were Oxygen, Sulfur, Chlorine, and Nitrogen. Other elements found in

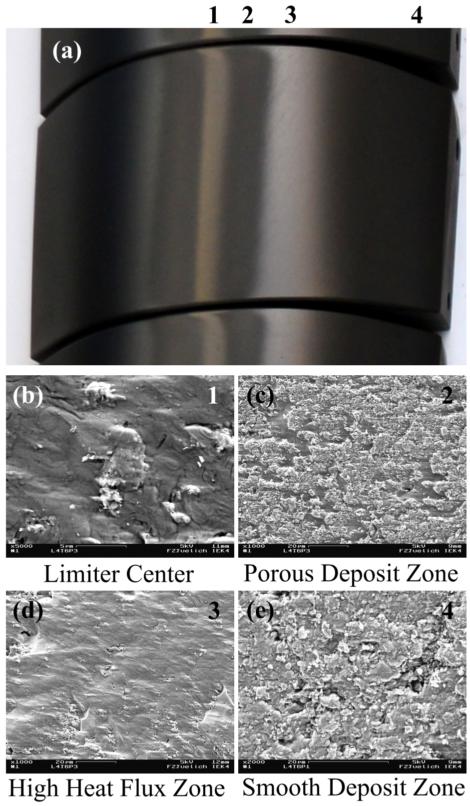

Figure 7. (a) A representative photograph of a limiter tile, with numbers corresponding to the numbers shown in 6. (b)-(d) Images of the surface of the tile in the four main interaction zones. The zone in which the images were taken are shown in the right corner of each image.

smaller quantities were Copper and Iron. Areas of pure Copper deposit were found near the bottom of some deposition regions, suggesting that larger amounts of Copper were ejected and deposited onto the limiter surface at the initial phase of the campaign or during conditioning with glow discharge, while only small amounts of Copper were eroded during the rest of the campaign.

4. Discussion and Future Work

A general overview of the PMI processes that occurred during the first operational campaign of W7-X was presented. All limiters contained the same four basic features: a smoothened center region, a rough deposit region, a pure erosion zone and then a smooth deposition region. The pure erosion zone found from materials analysis matches to the location where the high heat and particle fluxes were found via in-situ spectroscopy. In addition, the main impurities found in the deposits of the limiters (O, N, S, Cl) were confirmed to be found in the main plasma by other impurity diagnostics. It appears that large chunks of Copper were deposited onto the limiter surface at the beginning of the campaign and the reason for this is not yet known.

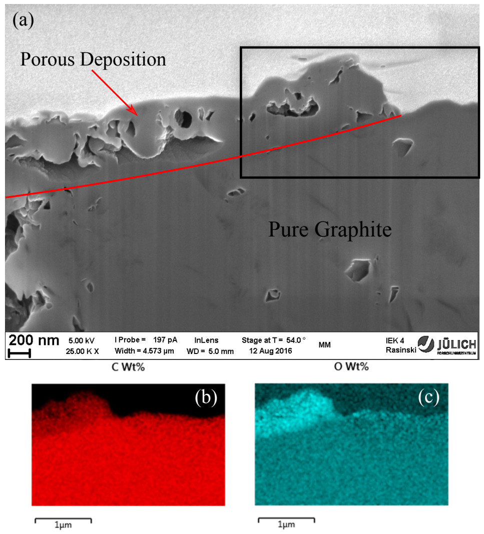

Figure 8. A FIB-cut cross-section of Limiter 4, Tile 6 (a). The boxed location in (a) was analyzed chemically using EDX. The deposition regions are characterized by a decrease in carbon content with a corresponding increase in oxygen content (b) and (c).

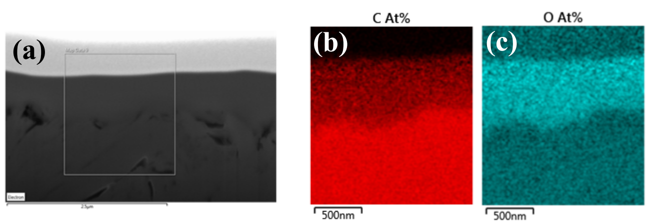

Figure 9. A FIB-cut cross section of a region closer to the edge of Limiter 4, Tile 6 (a). The boxed region in (a) was analyzed with EDX. The EDX chemical mapping, shown in (b) and (c) reveal that this smooth, dense region at the surface is a deposit.

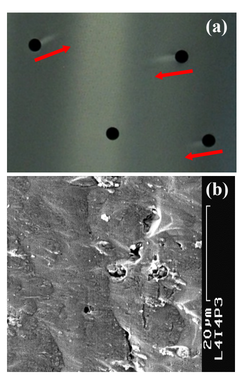

Figure 10. (a): Image of Limiter 5, Tile 7. The arrows indicate the direction of the eroded material coming off of the langmuir probes, which are overall pointed towards the center of the limiter. (b): An SEM image, tilted to the same orientation as the photograph on the right. The directionality of the features is horizontal.

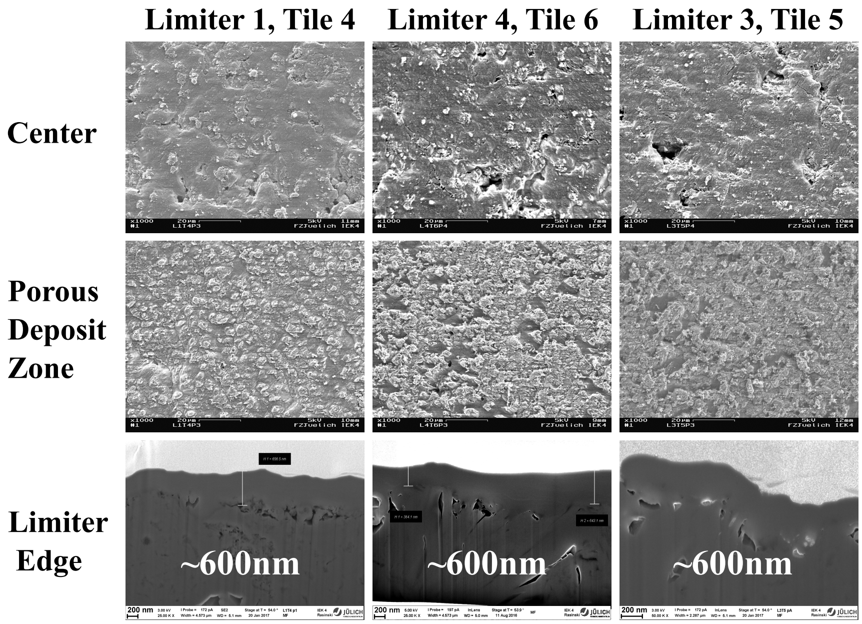

Figure 11. A comparison of tiles on three different limiters. Limiter 1 received the highest heat flux, while Limiter 3 received the lowest heat flux, comparatively. The features of all tiles are comparable, with comparable amounts of deposition on the edge of the tiles.

Currently, ERO analysis of the limiters is being conducted in order to confirm the underlying PSI physics processes that occurred during the first operational campaign. The processes outlined in this document rely on a simple 1D analysis of erosion from particle flux measurements and post-mortem materials analysis. With ERO, the full 3D plasma background can be taken into affect to see their full effects on the erosion and re-deposition as well as effects due to short and long range material migration. This modeling effort as well as further dedicated analyses will also be used to determine whether any 3D effects from the W7-X topology may be apparent under a closer inspection of the limiters. Future post-mortem analysis will include sections of tiles that showed strong left-right asymmetry in the heat flux, such as Limiter 3, Tile 3. This will be able to confirm whether there was a strong influence of the magnetic flux tube geometry poloidally on the PMI.

5. Acknowledgements

This work was supported in part by the U.S. Department of Energy under grants DE-SC00013911 and DE-SC00014210. The work has been carried out within the framework of the EUROfusion Consortium and has received funding from the Euratom research and training programme 2014-2018 under Grant Agreement No. 633053. The views and opinions expressed herein do not necessarily reflect those of the European Commission.

6. References

[1] J Roth, R Preuss, W Bohmeyer, S Brezinsek, A Cambe, E Casarotto, R Doerner, E Gauthier, G Federici, S Higashijima, J Hogan, A Kallenbach, A Kirschner, H Kubo, J M Layet, T Nakano, V Philipps, A Pospieszczyk, R Pugno, R Ruggiéri, B Schweer, G Sergienko, and M Stamp. *Nucl. Fusion*, 44:21–25, 2004.

[2] R Burhenn, Y Feng, K Ida, H Maassberg, K J McCarthy, D Kalinina, M Kobayashi, S Morita, Y Nakamura, H Nozato, S Okamura, S Sudo, C Suzuki, N Tamura, A Weller, M Yoshinuma, and B Zurro. *Nucl. Fusion*, 49, 2009.

[3] T Sunn Pedersen and et al. *Nucl. Fusion*, 55:126001, 2015.

[4] T Wauters, T Stange, Laqua H P, Marsen S, D Moseev, and O Volzke et al. In *Poster Presented at 43rd EPS Conference on Plasma Physics, Leuven*, 2016.

[5] F Effenberg, Y Feng, O Schmitz, H Frerichs, S A Bozhenkov, H Hölbe, R König, M Krychowiak, T Sunn Pedersen, D Reiter, L Stephey, and W7-X Team. *Nucl. Fusion*, 57, 2017.

[6] G A Wurden, C Biedermann, F Effenberg, M Jakubowski, H Niemann, L Stephey, S Bozhenkov, S Brezinsek, J Fellinger, B Cannas, F Pisano, S Marsen, H P Laqua, R König, O Schmitz, J H Harris, E A Unterberg, and W7-X team. *Nucl. Fusion*, 57, 2017.

[7] H Frerichs, F Effenberg, O Schmitz, C Biedermann, Y Feng, M Jakubowski, R König, M Krychowiak, J Lore, H Niemann, T S Pedersen, L Stephey, and G A Wurden. *Rev. Sci. Instr.*, 87:11D441, 2016.

[8] R. Koenig, J. Baldzuhn, and et al. *1st EPS Conference on Plasma Diagnostics*, 2015.

[9] G A Wurden, L A Stephey, C Biedermann, M W Jakubowski, J P Dunn, M Gamradt, and W7-X Team. *Review of Scientific Instruments*, 87, 2016.

[10] R J Colchin, D L Hillis, R Maingic C Kleppern H Brooks, R J Colchin, D L Hillis, and R Maingi. 2068:1–4, 2003.

[11] L Stephey, G A Wurden, O Schmitz, H Frerichs, F Effenberg, C Biedermann, J Harris, R König, P Kornejew, M Krychowiak, E A Unterberg, and W7-X Team. *Rev. Sci. Instr.*, 87, 2016.

[12] K. Behringer, H. P. Summers, B. Denne, M. Forrest, and M. Stamp. *Plasma Phys. Control. Fusion*, 31(14):2059–2099, 1989.

[13] S Brezinsek, G Sergienko, A Pospieszczyk, Ph Mertens, U Samm, and Greenland P T. *Plasma Phys. Control. Fusion*, 47:615–634, 2005.

[14] A Kirschner, A Kreter, P Wienhold, A Weckmann, A Pospieszczyk, R Ding, D Borodin, S Brezinsek, G Sergienko, M Rubel, Ch Linsmeier, and the TEXTOR team. *Nuclear Materials and Energy*, 2016.

[15] S Brezinsek and JET-EFDA contributors. *Journal Nucl. Mat.*, 463:11–21, 2015.

[16] G M Wright, A. A. Haasz, and et al. *J. Nucl. Mater.*, 337-339:74–78, 2005.

[17] C Li, N Gierse, J Oelmann, S Brezinsek, M Rasinski, C P Dhard, T Sunn Pedersen, R König, Y Liang, H Ding, C Linsmeier, and the W7-X team. *Physica Scripta*, 2017.

[18] Samuel A Lazerson, Matthias Otte, Sergey Bozhenkov, Marcin Jakubowski, and Ben Israeli. *Nucl. Fusion*, 57:8, 2017.